ISSN 1054-660X, Laser Physics, 2007, Vol. 17, No. 4, pp. 453–460.

Signal-to-Noise Analysis for Propagation of Laser Radiation through a Tissue-Like Medium by Diffuse Photon-Density Waves

U. J. Netz[a], A. H. Hielscher[b], A. K. Scheel[c], and J. Beuthan[a]

[a] *Department of Medical Physics and Laser Medicine, Charité–Universitätsmedizin Berlin, Fabeckstrasse 60-62, Berlin, 14195 Germany*

[b] *Departments of Biomedical Engineering and Radiology, Columbia University, ET351 Mudd Building, MC 8904, 500 West 120th Street, New York, NY 10027 United States*

[c] *Department of Medicine Nephrology and Rheumatology, Georg-August-University Göttingen, Robert-Koch-Strasse 40, Göttingen, 37075 Germany*

e-mail: uwe.netz@charite.de

Received October 19, 2006

Abstract—Biomedical optical imaging in the near-infrared (NIR) region provides the possibility to detect and determine pathological and functional changes in human tissue without the drawback of ionizing radiation. Of special promise is the application of this technology for the detection of joint diseases, such as rheumatoid arthritis (RA). It has been shown that optical changes in the synovial fluid and the vasculature surrounding the joints can be detected with optical methods. Applying optical tomographic methods one should be able to localize and quantify these changes for detection of the onset of RA. The first studies have been limited to continuous wave imaging. However, it is well known that enhanced resolution and better separation between absorption and scattering properties of tissue can be achieved using intensity modulated light sources. Intensity modulation of laser light in the MHz region leads to propagation of so-called diffuse photon density waves (PDW) through the tissue In this study we report on basic experimental results to determine performance and sensitivity of PDW-transillumination of tissue like phantoms. We used a vector network analyzer to generate and analyze intensity modulation from 100 MHz up to 1 GHz via a diode laser and an avalanche photo diode. Scans were performed across phantoms containing a layer with different absorbing and scattering properties bounded by an edge. The thickness of the phantoms was chosen similar to human fingers to gain information for optimization of tomographic imaging of finger joints. We experimentally determined the signal-to-noise ratio (SNR) of the system and compared the results to theoretical predictions. Noise and SNR of amplitude and phase depend on frequency of modulation. While the amplitude SNR decreases with frequency, phase SNR increases to assume a maximum value. We found that the inserted layer can be better characterized using phase information, which becomes more valuable as the source modulation frequency is increased. On the other hand, the sensitivity to perturbations is highest in the amplitude data obtained at lower frequencies. Thus, for tomographic imaging, optimal modulation frequencies should be found depending on the tissue type and nature of tissue inhomogeneities.

PACS numbers: 42.62.Be, 87.57.Ce, 87.63.Lk, 87.64.Cc, 87.66.Xa

DOI: 10.1134/S1054660X07040238

INTRODUCTION

In rheumatoid arthritis (RA), inflammatory changes (i.e., synovial proliferation) in finger joints offer a good possibility to obtain information on the state of the joint by light transmission measurements [1–5]. Using a diaphanoscopic method, it was possible to demonstrate in first clinical results that the inflammation stage can be evaluated [6, 7]. Representing the optical properties in a joint using an optical tomographic imaging process in comparison with an ultrasonic imaging process, it was possible to correctly evaluate the inflammation stage in primary diagnostics, too [8–10]. Despite the high photon scattering in the volume of the finger joint, a spatial resolution that would be sufficient for functional imaging should be obtained by optimization of the imaging process.

Studies up to now have been limited to continuous wave imaging (also called DC imaging), in which a light source is constantly switch on and the transmitted light intensities are measured at various positions. However, it is well known that so-called frequency domain measurement, in which the source intensity is sinusoidally modulated in the MHz range, can provide better resolution and better separation between absorption and scattering effects. The transmission of intensity-modulated light through diffusely scattering tissue can be described as propagation of a wave of modulated photon density, so-called photon density wave (PDW) [11]. Detection of phase and modulation (amplitude) of the waves delivers more information than a simple intensity measurement obtained with DC imaging systems. Therefore, transillumination by means of PDW is likely to improve both the detection of small differ-

ences in the optical properties and the specification of symptoms [12, 13].

In previous works, theoretical calculations and simulations were made to determine the resolving power of the PDW-based transillumination of tissue, and the results of experiments on phantoms were published relating to the detectability and characterization of inhomogeneities or of an edge spread function [14–18]. It turned out that the resolution generally increases with the frequency rising, which is mostly due to the increasing phase shift at higher frequencies. However, the noise, as given by the standard deviation in the amplitude and phase measurements, also increases with increasing frequency. Therefore, an optimum modulation frequency for maximum resolution and signal-to-noise ratio (SNR) should exist. This optimum frequency may differ depending on the tissue and the transillumination geometry, as for example shown by Boas et al. [14] in simulations studies, and by Toronov et al. [19] in simulations and experimental studies.

Basic experimental investigations on the resolution or SNR in the frequency domain have only been made up to a few hundred megahertz [19–21]. Investigations extending into the GHz domain were made via technically more demanding measurements in the time domain and subsequent Fourier transformation [19, 22]. However, this approach does not take into account the particular noise sources in frequency-domain measurements.

In a recently published study, we investigated PDW transillumination of small phantoms with high scattering and low absorbing properties [23]. We found a maximum in SNR at low frequencies, approximately 200 MHz.

Our experiments presented in this paper were aimed at analyzing signal-to-noise ratio in tissue-like material with finger joint-like properties depending on the PDW frequency and at investigating contrast by inhomogeneities inserted into the phantom. For this purpose, a frequency-domain measuring set-up was used covering a frequency domain from 100 MHz to 1 GHz. In particular, we studied phantoms with an inserted layer of varying absorbing and scattering properties.

MATERIAL AND METHODS

The propagation of the photon density as a wave in a homogeneous, infinite medium can be described in a short form as an equation that is composed of a DC and an AC part, i.e.,

$$\begin{aligned} J &= J_{\mathrm{DC}} + J_{\mathrm{AC}} \\ &= J_{\mathrm{DC}} + M\exp[i(kr - \omega t) - r\mu_{\mathrm{AC}}]. \end{aligned} \tag{1}$$

The first term on the right-hand side of (1) is the time-independent DC part and the second term is the time-dependent AC part of the wave. M stands for the modulation factor of the light, μ_{AC} for an effective AC attenuation coefficient, k for the wave vector, r for the path covered between the source and the detector, and $\omega = 2\pi f$ for the modulation angular frequency. $A = M\exp(-r\mu_{\mathrm{AC}})$ is the amplitude of the AC part, and the product kr is called the phase Φ of the wave. μ_{AC} and k depend primarily on the optical properties of the medium, i.e., absorption and scattering, and the frequency. The optical properties of scattering media are described by the reduced scattering coefficient μ_s' and the absorption coefficient μ_a.

Noise Models

The noise in optical signal measurement is caused by random fluctuation in dark signal (Johnson noise), in variation of the signal current of the photo detector (shot noise), and by other uncertainties, as for example positioning inaccuracy or source power fluctuation. For noise analysis, measurements are repeated and mean (signal) and standard deviation (noise) of signal fluctuation are calculated.

In experimental and theoretical investigations, Toronov et al. found that noise in PDW imaging mainly depends on shot noise [19]. The amplitude noise is proportional to the square root of the DC intensity and therefore independent of the frequency. The phase variations are also proportional to the square root of the DC intensity divided by the frequency-dependent amplitude:

$$\sigma_A(\omega) \sim \sqrt{\langle \mathrm{DC} \rangle}, \quad \sigma_\phi(\omega) \sim \frac{\sqrt{\langle \mathrm{DC} \rangle}}{\langle A(\omega) \rangle}. \tag{2}$$

The SNR is defined as

$$\mathrm{SNR}_A = \frac{\langle A_{\mathrm{signal}} \rangle}{\sigma_A} \tag{3}$$

for amplitude and in the same fashion for phase. This means that, according to Toronov et al., the frequency characteristic of amplitude SNR only depends on the amplitude behavior and phase SNR is influenced by phase and amplitude characteristic:

$$\begin{aligned} \mathrm{SNR}_A(\omega) &\sim \langle A(\omega) \rangle, \\ \mathrm{SNR}_\phi(\omega) &\sim \langle \phi(\omega) \rangle \langle A(\omega) \rangle. \end{aligned} \tag{4}$$

Boas et al. supposed in their theoretical considerations of the detection and characterization of inhomogeneities that the main sources of noise are shot noise and inaccuracies in the source and detector positions [14]. Considering changes in amplitude and phase due to perturbation by spherical scattering or absorbing inhomogeneities, they conclude that the amplitude noise caused by shot noise should rise approximately exponentially with the root from the frequency; while the positioning-error related noise increases circa linearly with the square root of the frequency. In the phase the shot noise rises exponentially with the frequency, while the noise due to positioning inaccuracies increases linearly with the square root of the frequency.

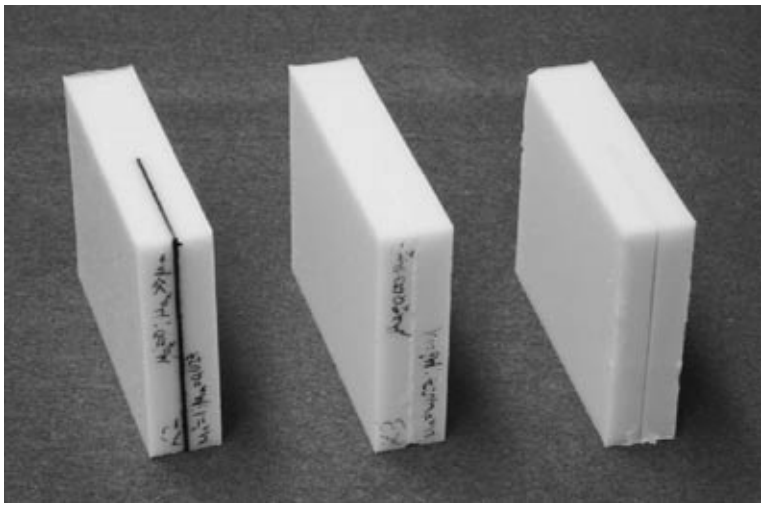

Fig. 1. Silicone phantoms with tissue-like properties and inserted layer.

Contrast

A sufficient contrast in images is important to distinguish between regions with different properties. The contrast due to the thin layer inserted in the phantoms is the difference of the signal before and behind the edge. The difference itself is not a good measure to investigate an imaging technique, because it depends on absolute values. Dividing the contrast by the noise leads to a contrast-to-noise ratio (CNR) that gives information about the sensitivity of the system to small perturbations,

$$\mathrm{CNR}_A = \frac{\delta A}{\sigma_{\delta A}} = \frac{\langle A_H \rangle - \langle A_L \rangle}{\sqrt{\sigma_H^2 + \sigma_L^2}}, \qquad (5)$$

where the subscripts H and L denote the homogeneous part and the part containing the layer, respectively. The definition for phase CNR is analogous.

Phantom

The phantoms were designed as a cuboid with thickness of 20 mm similar to typical finger thickness and with lateral dimensions high enough to avoid boundary problems in transillumination (x, y, z = 80, 70, 20 mm, Fig. 1). The material we used was silicone (Elastosil® RT 601, Wacker Chemie AG, Germany). This is a two-component material that is processed in the liquid phase before it hardens after some hours. Silicone is clear without significant absorption or scattering in the visible and near infrared spectrum with an index of refraction of n = 1.41. We added homogeneously distributed TiO_2 powder as scattering particles and a special silicone dye (Silopren LSR, GE Bayer Silicones, Germany). The tissue-like optical properties, i.e., absorption coefficient and reduced scattering coefficient of the phantom, were $\mu_a = 0.027$ mm^{-1} and $\mu_s' = 1.0$ mm^{-1} and were controlled by measurement with an integrating sphere system [24].

To investigate the sensitivity on small perturbations we inserted a 1 mm thin layer of the same material in the middle of three phantoms. This was done in a two step pouring process. The edge of the plane is located in the x direction in the middle of each phantom. The optical properties of the planes were adjusted that one plane is nearly totally absorbing and two planes have the bulk optical properties but doubled absorption or scattering, respectively (Table 1).

Experimental Set-Up

A vector network analyzer is used to modulate a diode laser (670 nm) and to analyse the RF signals from an avalanche photo diode (APD). Amplitude and phase of the AC signal are measured in the frequency range from 100 MHz up to 1 GHz (Fig. 2). The laser and detector system are both mounted on a stepping motor translation stage for coaxial scanning across the phantom surface. A computer serves as a control unit. A more detailed description of the experimental setup can be found elsewhere [23].

Optical properties of phantoms

	Scattering μ_s', mm^{-1}	Absorption μ_a, mm^{-1}
Bulk	1.0	0.027
Layer 1	1.0	12
Layer 2	2.0	0.027
Layer 3	1.0	0.054

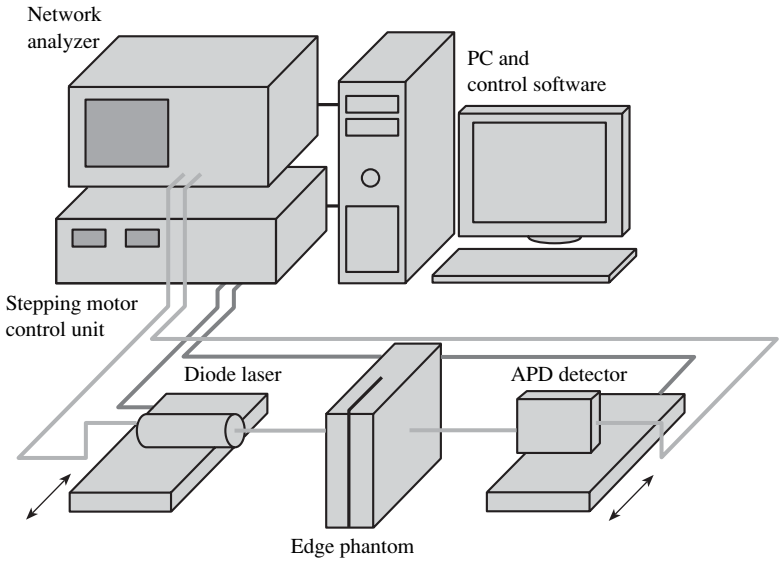

Fig. 2. Experimental setup for scanning amplitude and phase measurement.

Calibration

The network analyzer uses the modulation at the output internally as a reference to the input signal. The measured values are the amplitude A relative to the modulation power at the output and the relative phase Φ in the range $[-\pi, \pi]$. Besides the transmission characteristic of the transilluminated phantom, these measured values also contain the attenuation and phase shift of the optical and electrical system, i.e.,

$$J_{\text{measured}} = A_{\text{phantom}} A_{\text{system}} \exp[i(\phi_{\text{phantom}} + \phi_{\text{system}} - \omega t)]. \quad (6)$$

To determine only the phase shift and the relative amplitude attenuation caused by the phantom, the transmission behavior of the system is to be determined as calibration in a first step. For this purpose, the light is attenuated by a neutral density filter instead of the phantom. Since the filter contribution to the phase shift is negligible, the measured phase is equal to the phase shift generated by the system. The filter does only damp the intensity by constant factor and has no influence on the frequency spectrum. The amplitude spectrum after the filter thus reflects the system part of the AC attenuation multiplied by the filter transmission factor F:

$$J_{\text{calibration}} = F A_{\text{system}} \exp[i(\phi_{\text{system}} - \omega t)]. \quad (7)$$

The correction is done by dividing the phantom measurement by the calibration measurement:

$$J_{\text{phantom}} = \frac{J_{\text{measured}}}{J_{\text{calibration}}} = \frac{1}{F} A_{\text{phantom}} \exp(i\phi_{\text{phantom}}) = A'_{\text{phantom}} \exp(i\phi_{\text{phantom}}). \quad (8)$$

Measurement

Prior to each measurement, the system's dark signal was measured and subtracted from the measured data. For the calibration measurement, a combination of two filters was used which jointly featured a transmission of 3.6×10^{-4} at 670 nm. The laser and the detector system were coaxially scanned over the phantom in 1-mm increments in the x direction at half the y height over a range from –15 to 15 mm relative to the edge position, starting in the homogeneous part. At each position the laser was modulated over a frequency range from 100 MHz to 1 GHz in increments of 50 MHz and the amplitude and phase were determined. The measurements of dark signal, calibration, and the complete scanning of the phantom each were repeated 10 times for statistical signal analysis.

After signal correction by the calibration measurement, the phase is corrected by 2π at phase jumps so that there is a constant phase course. The total amplitude and phase uncertainty thus consists of the dark signal, the measurements, and the calibration.

RESULTS

Dark Signal

The dark signal reflects the frequency characteristic of the electronic fluctuations of the complete system without light. The phase is affected by noise over the total range of $[-\pi, \pi]$. Towards 1000 MHz the amplitude increases slightly with some characteristic peaks in the spectrum, the phase jitter diminishes a little. These are systematic errors and are caused by the modulation input of the laser acting more and more as an emitter with the frequency increasing. Therefore, the

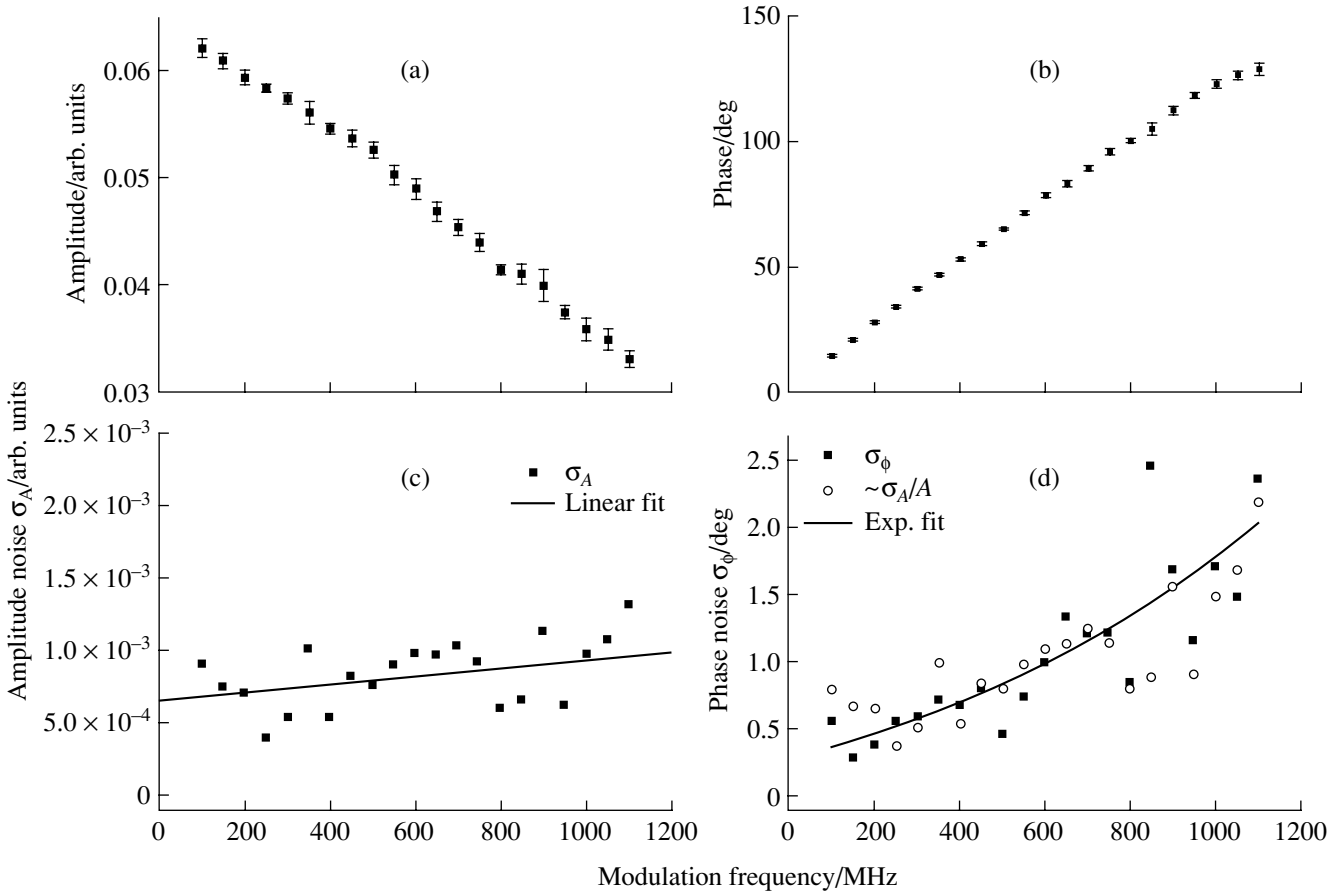

Fig. 3. (a) Amplitude and (b) phase in the homogeneous part of the phantom vs. modulation frequency, (c) noise of amplitude with linear fit and (d) phase noise with fitted data according to theory by Toronov et al. (circle) and exponential fit.

detection system is subjected to an electromagnetic distortion by the RF signal.

Homogeneous Part of Phantoms

The frequency behavior of amplitude and phase is represented in Figs. 3a and 3b. With increasing modulation frequency, the amplitude decreases, and the phase starts increasing approximately linearly with the modulation frequency with a slight saturation to higher frequencies.

In our experiments, the positioning error is on the order of micrometers and can therefore be neglected. The amplitude noise is almost constant but shows a slight increase with frequency (Fig. 3c). The phase noise increases to higher frequencies, about nearly proportionally to σ_A/A or to an exponential fit (Fig. 3d). Thus, our experimental data rather correspond to the theoretical results predicted by Toronov et al. in Eq. (2).

The amplitude SNR in Fig. 4a decreases somewhat faster than the best fit by the amplitude according to (4). There seems to be a maximum around 200 MHz. The phase SNR clearly rises with frequency (Fig. 4b). It shows some kind of saturation above 800 MHz. The product of phase and amplitude fitted in these data shows a maximum around 900 to 1000 MHz.

Scanning the Edge

Approaching the totally absorbing edge at scanning the phantom, the normalized amplitude $A_{\text{norm}} = A/\max\{A\}$ starts getting smaller and drops behind the edge (Fig. 5a). In the curves, no clear dependence on frequency is visible up to 1000 MHz. While the phase gets smaller close to the edge, it quickly rises behind it. The minimum is a few millimeters before the edge. With the frequency increasing, in the shifted phase $\Phi_{\text{shift}} = \Phi - \Phi_{x=0}$ a more distinct minimum and a steeper increase behind the edge can be seen (Fig. 5b).

The phantoms with increased scattering or absorption in the layer, respectively, show that the amplitude drops a little towards and behind the edge due to the increased attenuation and the phase increases or decreases, respectively. The contrast is calculated by taking the signal difference at 10 mm before and 10 mm behind the edge. The dependence on the frequency is depicted in Fig. 6. The data seems to be very noisy above 400 MHz, but these deviations show a structure

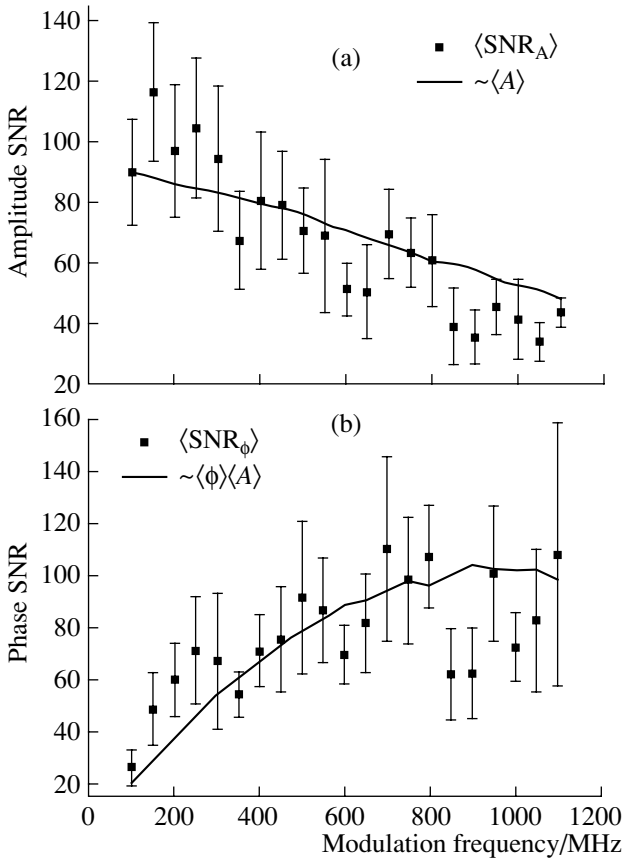

Fig. 4. Signal-to-noise ratio of (a) amplitude and (b) phase with fit according to theory, mean and standard deviation over 10 *x*-positions.

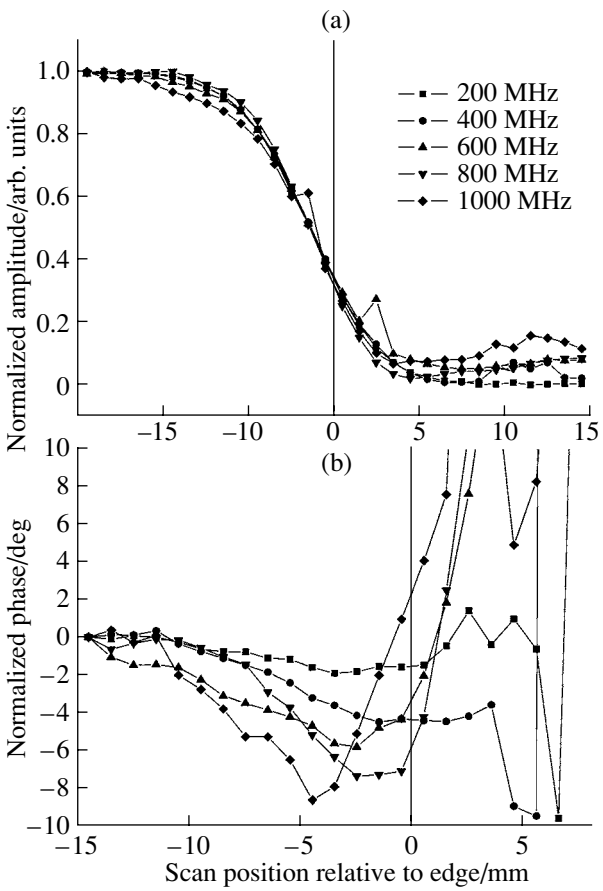

Fig. 5. Coaxial scan over the totally absorbing edge: (a) amplitude and (b) phase for different frequencies, normalized to position $x = -15$ mm.

in the frequency spectrum and are probably caused by electromagnetic RF distortion from the RF laser modulation. Nevertheless, the trend of the data shows that amplitude contrast is almost constant and nearly the same for the absorbing and scattering layer. In phase, the contrast is positive for scattering and negative for the absorbing layer. The absolute values increase with the frequency. The contrast at the scattering layer is a little higher than at the absorbing one.

The CNR of the amplitude decreases with increasing frequency in the same fashion for both inserted planes. The absolute value of the phase CNR increases with the frequency but also behaves very noisily above 400 MHz.

DISCUSSION

Signal and noise analysis show that both amplitude and phase show some kind of maximum in SNR, around 200 MHz for amplitude and above 800 MHz in phase. In former studies, in which we used stronger scattering and less absorbing phantoms, we found different SNR characteristic in amplitude and phase: both showed a maximum around 200 MHz [23]. Considering the SNR, Toronov et al. investigated changes due to absorbing inhomogeneities in the human brain by Monte Carlo simulation. They found a maximum in the phase SNR between 300 to 500 MHz. According to Boas et al., who looked at photon density waves in a 6-cm thick slab, SNR of changes due to absorbing inhomogeneities regresses steadily to high frequencies. When detecting scattering inhomogeneities, however, the phase SNR reaches a maximum at about 500 MHz. The amplitude SNR falls off steadily.

In PDW transillumination, amount and the frequency characteristic of amplitude damping and phase depend on the optical properties. Therefore, it is not surprising that studies with different optical properties show different characteristic and different frequencies with optimal SNR. Scanning of the edge shows a characteristic signal response. The contrast analysis for detection of small layers with doubled absorption or scattering compared to the bulk medium shows different behaviour for amplitude and phase. Contrast in amplitude seems to be the same for absorption and scattering perturbation. It shows no clear frequency dependence, whereas amplitude CNR clearly decreases toward higher frequencies. However, phase contrast

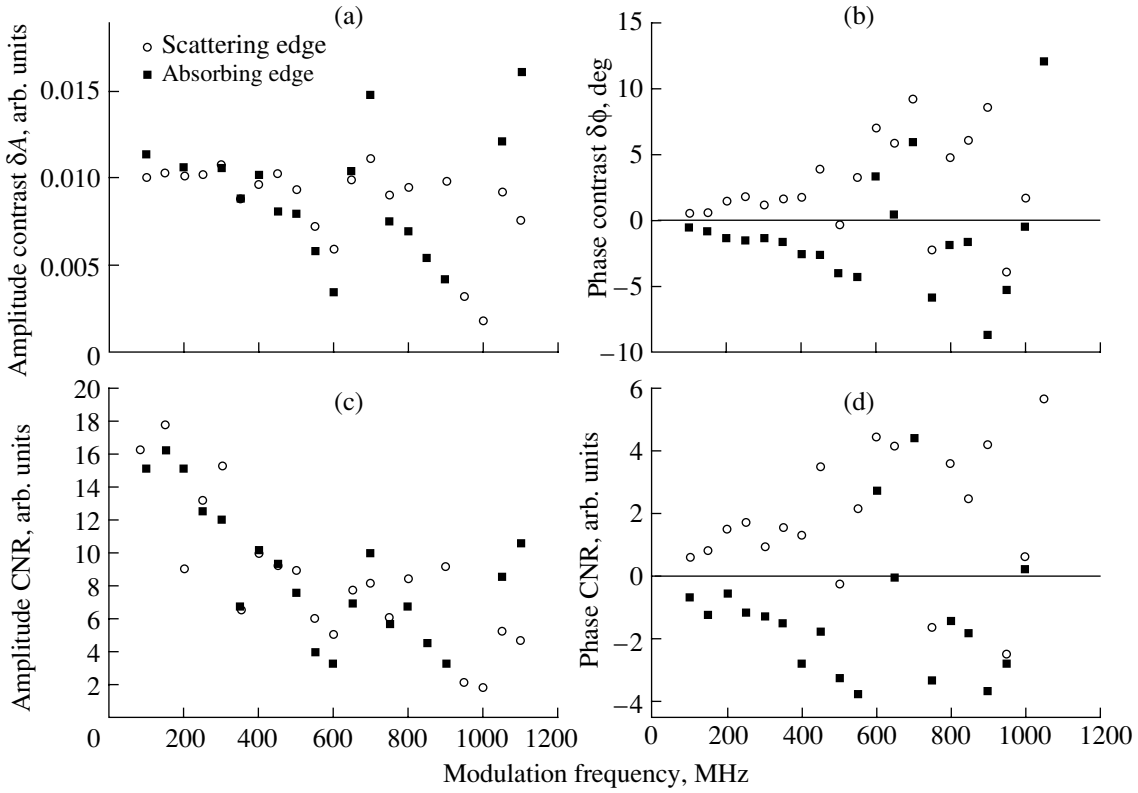

Fig. 6. Contrast in (a) amplitude and (b) phase of absorbing (square) and scattering (circle) layer, contrast-to-noise ratio of (c) amplitude and (d) phase.

and CNR clearly increases with frequency having opposite sign for the absorbing and scattering layer. In the investigated frequency range, phase CNR is well below amplitude CNR and reaches 1 at higher frequencies only. Therefore, at low frequencies, sensitivity is better in the amplitude signal, whereas phase gets more sensitive with higher frequency. Characterization of the kind of perturbation is better in phase than in amplitude.

CONCLUSIONS AND OUTLOOK

The frequency dependence of noise and SNR in our frequency domain experiments are in good agreement to theoretical predictions. Amplitude and phase SNR have maximum values but at opposite sites of the frequency range from 100 MHz to 1 GHz covered in our measurements. The characterization of perturbations is better in phase signal than in amplitude whereas amplitude CNR and therefore the sensitivity is better in the amplitude signal. Here we see the same trend in the frequency characteristic as for signal-to-noise analysis, i.e., better phase CNR and worse amplitude contrast toward higher frequencies.

We conclude that, for PDW imaging, in general it would be useful to choose a single frequency around 500 MHz, not too low for good phase signal and not too high for high amplitude SNR. For enhanced imaging results, it would be better to use at least two frequencies for separated amplitude and phase analysis.

For imaging of finger joints and particularly for tomographic reconstruction of the optical properties in finger joints, the use of both amplitude and phase should decisively improve sensitivity and contrast compared to conventional intensity measurements. Future experiments with phantoms providing in more detail the anatomic structure and specific optical properties of finger joints should show how sensibly a frequency domain reconstruction method is to spatial changes of the optical properties as they occur in joint diseases.

ACKNOWLEDGMENTS

This work was supported by grant R01 AR46255 from the National Institute of Arthritis and Musculoskeletal and Skin Diseases (NIAMS), USA, which is part of the National Institutes of Health.

REFERENCES

1. J. Beuthan, O. Minet, G. Müller, and V. Prapavat, in *Medical Optical Tomography: Functional Imaging and Monitoring*, Ed. by G. Müller, B. Chance, R. Alfano, et al. (SPIE, Bellingham, Washington, 1993), p. 263.
2. V. Prapavat, W. Runge, A. Krause, et al., Minimal Invasive Med. **8** (1–2), 7 (1997).

3. Y. Xu, N. Iftimia, H. Jiang, et al., Opt. Express **8**, 447 (2001).
4. J. Beuthan, U. Netz, O. Minet, et al., Quantum Electron. **32**, 945 (2002).
5. Y. Xu, N. Iftimia, H. Jiang, et al., J. Biomed. Opt. **7**, 88 (2002).
6. A. K. Scheel, A. Krause, I. Mesecke-von Rheinbaben, et al., Arthritis Rheum. **46**, 1177 (2002).
7. A. Schwaighofer, V. Tresp, P. Mayer, et al., IEEE Trans. Biomed. Eng. **50**, 375 (2003).
8. A. D. Klose and A. H. Hielscher, Med. Phys. **26**, 1698 (1999).
9. A. H. Hielscher, A. Klose, A. K. Scheel, et al., Phys. Med. Biol. **49**, 1147 (2004).
10. A. K. Scheel, M. Backhaus, A. D. Klose, et al., Ann. Rheum. Dis. **64**, 239 (2005).
11. J. B. Fishkin, E. Gratton, M. J. VandeVen, and W. W. Mantulin, Proc. SPIE **1431**, 122 (1991).
12. S. R. Arridge and W. R. B. Lionheart, Opt. Lett. **23**, 882 (1998).
13. S. R. Arridge, Inverse Probl. **15**, R41 (1999).
14. D. A. Boas, M. A. O'Leary, B. Chance, and A. G. Yodh, Appl. Opt. **36**, 75 (1997).
15. J. B. Fishkin and E. Gratton, J. Opt. Soc. Am. **10**, 127 (1993).
16. H. Wabnitz and H. Rinneberg, Appl. Opt. **36**, 64 (1997).
17. J. Beuthan, V. Prapavat, R. Naber, et al., Proc. SPIE **2676**, 43 (1996).
18. I. Mesecke-von Rheinbaben, A. Roggan, J. Helfman, et al., Proc. SPIE **3601**, 482 (1999).
19. V. Toronov, E. D'Amico, D. Hueber, et al., Opt. Express **11**, 2717 (2003).
20. M. S. Patterson, B. W. Pogue, and B. C. Wilson, in *Medical Optical Tomography: Functional Imaging and Monitoring*, Ed. by G. Müller, B. Chance, R. Alfano, et al. (SPIE, Bellingham, Washington, 1993), p. 513.
21. L. Montandon, D. Salzmann, F. Bevilacqua, and C. Depeursinge, Proc. SPIE **3566**, 236 (1998).
22. J. B. Fishkin, S. Fantini, M. J. VandeVen, and E. Gratton, Phys. Rev. E **53**, 2307 (1996).
23. U. J. Netz, A. H. Hielscher, A. K. Scheel, and J. Beuthan, Laser Phys. **16**, 765 (2006).
24. A. Roggan, O. Minet, C. Schrönder, and G. Müller, in *Medical Optical Tomography: Functional Imaging and Monitoring,* Ed. by G. Müller, B. Chance, R. Alfano, et al. (SPIE, Bellingham, Washington, 1993), p. 149.